# The Leafless Orchid Cymbidium macrorhizon Performs Photosynthesis in the Pericarp during the Fruiting Season

| メタデータ | 言語: eng |
| --- | --- |
| | 出版者: |
| | 公開日: 2022-04-18 |
| | キーワード (Ja): |
| | キーワード (En): |
| | 作成者: Kobayashi, Koichi, Suetsugu, Kenji, Wada, Hajime |
| | メールアドレス: |
| | 所属: |
| URL | http://hdl.handle.net/10466/00017656 |

1    *Title:*

2    **The leafless orchid *Cymbidium macrorhizon* performs photosynthesis in pericarp**

3    **during fruiting season**

4

5    *Running head:*

6    Photosynthesis in a leafless orchid

7

8    *Authors:*

9    Koichi Kobayashi[1*], Kenji Suetsugu[2] and Hajime Wada[3]

10

11    *Authors' Addresses:*

12    [1]Faculty of Liberal Arts and Sciences, Osaka Prefecture University, 1-1 Gakuen-cho,

13    Naka-ku, Sakai, Osaka, 599-8531 Japan

14    [2]Department of Biology, Graduate School of Science, Kobe University, 1-1 Rokkodai,

15    Nada-ku, Kobe, 657-8501, Japan

16    [3]Department of Life Sciences, Graduate School of Arts and Sciences, The University of

17    Tokyo, Komaba 3-8-1, Meguro-ku, Tokyo 153-8902, Japan

18

19    *Corresponding Author

20    ***Abstract***

21    Photosynthesis with highly photoreactive chlorophyll (Chl) provides energy for plant

22    growth but with simultaneous risk of photooxidative damage and photoprotection costs.

23    Although the leafless orchid *Cymbidium macrorhizon* mostly depends on mycorrhizal

24    fungi for carbon, it accumulates Chl particularly during fruiting and may not be fully

25    mycoheterotrophic. In fact, stable isotopic analysis suggested that the fruiting *C.*

26    *macrorhizon* specimens obtain a significant proportion of its carbon demands through

27    photosynthesis. However, actual photosynthetic characteristics of this leafless orchid are

28    unknown. To reveal the functionality of photosynthetic electron transport in *C.*

29    *macrorhizon*, we compared its photosynthetic properties with those of its relative

30    mixotrophic orchid *C. goeringii* and the model plant *Arabidopsis thaliana*.

31        Compared with *C. goeringii* and *A. thaliana*, maximum photochemical efficiency of

32    PSII was substantially low in *C. macrorhizon*. Chl fluorescence induction kinetics

33    revealed that the electron transport capacity of PSII was limited in *C. macrorhizon*. Chl

34    fluorescence analysis at 77K suggested partial energetic disconnection of the light-

35    harvesting antenna from the PSII reaction center in *C. macrorhizon*. Despite its low PSII

36    photochemical efficiency, *C. macrorhizon* showed photosynthetic electron-transport

37    activity both in the field and under laboratory conditions. *C. macrorhizon* developed

38    strong non-photochemical quenching in response to increased light intensity as did *C.*

39    *goeringii*, suggesting the functionality of photoprotective systems in this orchid.

40    Moreover, *C. macrorhizon* fruit developed stomata on the pericarp and showed net $O_2$-

41    evolving activity. Our data demonstrate that *C. macrorhizon* can perform photosynthetic

42    electron transport in the pericarp, although its contribution to net carbon acquisition may

43    be limited.

44

48

***Introduction***

Most plants grow photoautotrophically by using atmospheric $CO_2$ as their sole carbon

source, but several chlorophyllous species in Orchidaceae obtain carbon from

mycorrhizal fungi in addition to assimilating $CO_2$ by photosynthesis (reviewed by Selosse

and Roy, 2009). For example, *Cymbidium goeringii* can obtain 30% to 50% of its carbon

from its mycorrhizal fungi (Motomura et al., 2010). Meanwhile, some orchids completely

lack chlorophyll (Chl) and photosynthetic capability, thus fully depending on associated

fungi for their carbon source. Many of these fully mycoheterotrophic orchids grow

underground for most of their life cycle (Leake, 1994). Besides these achlorophyllous

orchids, some orchids lack foliage leaves but accumulate Chl in shoots or roots (Cameron

et al., 2009; Zimmer et al., 2008). Zimmer et al. (2008) reported that *Corallorhiza trifida*,

with leaves reduced to scales, accumulates Chl and retains some potential for autotrophic

activity. On the basis of the isotope mixing model that assumes a linear correlation

between the carbon gain from fungi and the enrichment of $^{13}C$ to define the heterotrophic

levels of autotrophic (0% organic nutrient gain from fungi) and fully mycoheterotrophic

(100% nutrient gain from fungi) plants (Gebauer and Meyer, 2003), the authors estimated

that ~33% of the total carbon source is from autotrophic activity in *C. trifida*. In fact,

Cameron et al. (2009) used Chl fluorescence analysis to reveal that *C. trifida* shoots had

reduced but significant capability of the photochemical reaction of PSII. However, direct

measurement of the potential for $CO_2$ assimilation in the field indicated that *C. trifida* was in a nutritional mode close to fully mycoheterotrophic under field conditions (Cameron et al., 2009). The authors proposed that *C. trifida* is at a late stage in the evolutionary development toward complete mycoheterotrophy. However, these results deviated from those of an older study (Montfort and Küsters, 1940) reporting that the $CO_2$ assimilation of *C. trifida* inflorescence and infructescence was 2.2 times higher than the level of respiration.

The orchid *Cymbidium macrorhizon* does not develop normal leaves and is often assumed to be fully mycoheterotrophic (Motomura et al., 2010; Ogura-Tsujita et al., 2012). However, this species accumulates Chl in the shoot particularly during fruiting. Linear two-source mixing model analysis of $^{13}C$ and $^{15}N$ revealed that fruiting *C. macrorhizon* plants obtain ~75% of their total carbon from their mycorrhizal fungi (Suetsugu et al., 2018). The data indicate that this species is not fully mycoheterotrophic and would fix a certain proportion of their carbon from the atmosphere at least during the fruiting stage. By contrast, *C. goeringii*, a close relative of *C. macrorhizon*, produces fully expanded leaves and grows mixotrophically depending on associated fungi for 30% to 50% of its carbon (Motomura et al., 2010).

To understand how the photosynthetic apparatus functions in chlorophyllous but highly mycoheterotrophic orchids, we compared photosynthetic properties of *C. macrorhizon* with those of mixotrophic *C. goeringii* and fully autotrophic *Arabidopsis thaliana*. Our data indicate that *C. macrorhizon* performs the photochemical and photosynthetic electron transport in the pericarp, although the maximum quantum efficiency of PSII is low.

92    *Results*

93    ***C. macrorhizon* accumulates photosynthetic pigments during the fruiting stage**

94    Pericarps of *C. macrorhizon* were pale-green at the flowering stage, but the green color

95    deepened during fruit maturation (Fig. 1). Pigments extracted from mature *C.*

96    *macrorhizon* pericarp with 80% acetone showed an absorption spectrum typical of that

97    from photosynthetic tissues containing Chls and carotenoids, as represented by spectra

98    from *A. thaliana* leaves and pericarps (Fig. S1). However, pigments from *C. macrorhizon*

99    pericarp had higher absorption, around 650 nm and 470 nm, than those from *A. thaliana*

100   leaves and pericarps, which indicates relatively high accumulation of Chl *b* and

101   carotenoids in *C. macrorhizon* pericarp. In fact, ratios of Chl *a* to Chl *b* and carotenoids

102   were lower in *C. macrorhizon* pericarp and stems than in leaves and pericarp of *A.*

103   *thaliana* (Fig. S1, Table 1). Moreover, total Chl content in the pericarp of *C. macrorhizon*

104   was ~90% lower than that of *A. thaliana* on a fresh weight basis. The Chl content and Chl

105   *a*/*b* ratio in pericarp were also lower in *C. goeringii* than *A. thaliana*, whereas Chl content

106   in leaves was similar between these two plants.

107       Because the dry weights of *C. macrorhizon* pericarp and stem after pigment

108   extraction were 9.1 ± 1.2% and 12.7 ± 1.8 % (mean ± SD, n = 9) of their fresh weight,

109   respectively, and these values were similar to those in *A. thaliana* leaves (9.0 ± 0.8%), the

110   lower pigment levels in *C. macrorhizon* were not attributed to high water content in these

111   tissues. By regarding the *C. macrorhizon* fruit as an ellipsoid, its surface area and volume

112   can be roughly estimated around 500 mm$^2$ and 600 mm$^3$, respectively, from its average

113   length (30.1 mm, SD = 1.7, n = 4) and width (6.3 mm, SD = 0.7, n = 4). This estimation

114   was supported by the actual measured volume of mature *C. macrorhizon* fruits (566.3

115   mm$^3$, SD = 115.8, n = 4). Because the total Chl content per a mature *C. macrorhizon* fruit

116    was 56.1 nmol (SD = 11.9, n = 4), Chl content of *C. macrorhizon* fruit can be roughly

117    estimated as ~0.1 nmol mm$^{-2}$, which was lower than those in *A. thaliana* leaves (0.37

118    nmol mm$^{-2}$, SD = 0.02, n = 4).

119

120    **Reduced photosynthetic efficiency in *C. macrorhizon***

121    To assess whether *C. macrorhizon* has potential to perform photosynthesis, we compared

122    maximum quantum yield (Fv/Fm) of PSII in *C. macrorhizon* with that in *A. thaliana* and

123    *C. goeringii* (Table 1). In *A. thaliana* and *C. goeringii*, Fv/Fm was only slightly lower in

124    the pericarp than leaves. By contrast, in *C. macrorhizon*, Fv/Fm was remarkably low in

125    both stems and pericarp. Imaging analysis of Chl fluorescence revealed that mature *C.*

126    *macrorhizon* fruit showed relatively high minimal Chl fluorescence (Fo) compared with

127    *C. goeringii* and *A. thaliana* leaves (Fig. 2), although fruits of *C. goeringii* and *A. thaliana*

128    showed similar Fo levels compared with leaves of respective plants (Fig. S2).

129        To further characterize the functionality of the photosynthetic machinery, we

130    analyzed the quantum yield of PSII ($Y_{II}$) and that of regulated ($Y_{NPQ}$) and non-regulated

131    ($Y_{NO}$) energy dissipation under increased actinic light intensity (Fig. 3 and Fig. S3). $Y_{II}$

132    represents the fraction of light energy used for photosynthetic reactions, whereas $Y_{NPQ}$

133    and $Y_{NO}$ correspond to the fraction of energy thermally dissipated via the light-induced

134    photoprotective mechanism and that passively dissipated mainly in the form of

135    fluorescence, respectively (Kramer et al., 2004). Of the three plant species investigated

136    (*C. macrorhizon*, *C. goeringii* and *A. thaliana*), *C. macrorhizon* showed lowest $Y_{II}$ and

137    highest $Y_{NPQ}$ levels in the pericarp under all actinic light intensities, followed by *C.*

138    *goeringii*. Based on the "puddle" model (Kramer et al., 2004), $Y_{II}$ can be viewed as a

139    product of two components, the coefficient of photochemical quenching (qP), which

6

140 represents the redox status of the primary electron acceptor ($Q_A$) of PSII and thus the

141 openness of PSII, and the maximum quantum efficiency of open PSII (Fv'/Fm'). In *C.*

142 *macrorhizon* pericarp, Fv'/Fm' was substantially low as compared with other two plants

143 (Fig. 3D), whereas qP levels were not largely different from those in *C. goeringii* pericarp

144 (Fig. 3E). In contrast to the continuous increase of the relative electron transport rate

145 (rETR) in *A. thaliana* in response to increased actinic light intensity, rETR was saturated

146 at lower light in *C. macrorhizon* and *C. goeringii* (Fig. 3F). In *C. macrorhizon*, light

147 response curves of these parameters were similar between stems and pericarp (Fig. S3),

148 so these profiles are typical features of green tissues in *C. macrorhizon*. Similarly, *A.*

149 *thaliana* showed similar light response patterns between leaves and pericarps, whereas *C.*

150 *goeringii* leaves and pericarps showed some differences in these parameters (Fig. S3).

151 To address whether *C. macrorhizon* can perform photosynthesis in their habitat, we

152 analyzed $Y_{II}$ in pericarp tissue of six *C. macrorhizon* individuals under natural light

153 conditions in an evergreen forest dominated by *Quercus glauca* in October 2016 (Fig.

154 3G). In these samples, $Y_{II}$ levels ranged from 0.12 to 0.42 under varying sunlight

155 intensities between 50 and 120 μmol photons $m^{-2}$ $s^{-1}$. The result was consistent with the

156 light curve data for $Y_{II}$ under laboratory conditions (Fig. 3A). Thus, *C. macrorhizon*

157 pericarp can perform photosynthetic electron transport under natural growth conditions.

158

159 ***C. macrorhizon* pericarp shows limited electron transport capacity of PSII**

160 To evaluate electron transport activity in *C. macrorhizon*, we analyzed the fast induction

161 kinetics of Chl fluorescence (Fig. 4A). With actinic illumination, *A. thaliana* leaves and

162 fruits, which were used as typical photosynthetically competent examples, showed a

163 gradual increase in Chl fluorescence, reflecting the high electron transport activity from

164 PSII to PSI. Similar kinetics were observed in *C. goeringii* leaves (Fig. S4A). By contrast,

165 in *C. macrorhizon* fruits, Chl fluorescence was strongly increased at the fast phase of the

166 induction kinetics, probably because of the limited electron-transfer capability in PSII.

167 　　To further dissect the electron transport activity of PSII in *C. macrorhizon*, we

168 analyzed decay curves of single flash-induced Chl fluorescence (Fig. 4B), which reflects

169 reoxidation kinetics of $Q_A$ in PSII (Krause and Weis, 1991). As for *A. thaliana* leaves and

170 fruits, *C. macrorhizon* fruits showed fast fluorescence decay after flash irradiation, which

171 suggests no retardation of electron transfer from $Q_A^-$ to the secondary electron acceptor

172 ($Q_B$) at the PSII acceptor side. *C. goeringii* leaves also showed $Q_A$ reoxidation kinetics

173 similar to *A. thaliana* leaves (Fig. S4B).

174

175 **Photosystem complexes in *C. macrorhizon* pericarp**

176 To examine the state of photosystem complexes in *C. macrorhizon* pericarp, we measured

177 Chl fluorescence spectra from membrane fractions at 77K (Fig. 5). The membrane

178 fraction of *A. thaliana* leaves showed 2 major emission bands peaking around 730 ($F_{PSI}$)

179 and 682 nm ($F_{PSII}$), originating from PSI and PSII complexes, respectively (Krause and

180 Weis, 1991). In *C. goeringii* leaves, the peak of $F_{PSI}$ was observed at 735 nm along with

181 the peak of $F_{PSII}$ at 682 nm and the mean $F_{PSII}/F_{PSI}$ ratio with SD ($1.41 \pm 0.09$, n = 3) was

182 higher than that in *A. thaliana* ($0.75 \pm 0.07$, n = 6) (Fig. S4C). As for these

183 photosynthetically competent leaves, two emission bands were observed in *C.*

184 *macrorhizon* membranes, although the $F_{PSII}$ peak was slightly blue-shifted to ~680 nm,

185 with the $F_{PSI}$ peaking at 735 nm (Fig. 5). Moreover, the $F_{PSII}/F_{PSI}$ ratio was notably high

186 in *C. macrorhizon* ($2.59 \pm 0.54$, n = 6). These features were consistently observed between

187 younger and older fruits of a *C. macrorhizon* plant (Fig. S5).

188

**189** ***C. macrorhizon* fruit evolves $O_2$ in a light-dependent manner and develops stomata**

**190** **on the pericarp**

191   To assess whether *C. macrorhizon* fruit can photosynthetically generate $O_2$, we

192   determined $O_2$-evolving activity in whole intact fruit of *C. macrorhizon* in a closed air

193   chamber with the atmospheric $CO_2$ concentration (Fig. 6A). Although *C. macrorhizon*

194   fruit consumed $O_2$ by respiration in darkness, the fruit slightly evolved $O_2$ under 50 µmol

195   $m^{-2} s^{-1}$ light. $O_2$ evolution from *C. macrorhizon* fruit was further enhanced with increased

196   light intensity.

197        Because *C. macrorhizon* is reported to have degenerated stomata on scale leaves

198   (Yukawa and Stern, 2002), we examined whether *C. macrorhizon* fruits have stomata on

199   the pericarp. In scanning electron microscopy (SEM) analysis, we observed stomatal

200   development on *C. macrorhizon* pericarp surfaces in a density of 17.6 $mm^{-2}$ (SD = 4.9, n

201   = 3) (Fig. 6B-D). Light microscopy analysis of pericarp sections revealed that stomata of

202   the *C. macrorhizon* pericarp have no or underdeveloped substomatal chambers (Fig. 6E).

203   However, large parenchyma cells containing chloroplasts were present below the stomata,

204   possibly to exchange gases through the cells via free diffusion.

205

**206** ***Discussion***

**207** **Green tissues of *C. macrorhizon* possess photosynthetic electron transport activity**

208   Our data show that *C. macrorhizon* pericarp and stem accumulate photosynthetic

209   pigments and perform photosynthetic electron transport, although the maximum quantum

210   efficiency of PSII photochemistry is substantially low (Fig. 3 and Table 1). Moreover, we

211   detected light-dependent $O_2$ evolution from *C. macrorhizon* fruit (Fig. 6A) and stomata

development on the pericarp (Fig. 6B-E). Thus, green tissues of *C. macrorhizon* maintain functional photosynthetic machinery and can perform photosynthesis under light. In fact, *C. macrorhizon* pericarp showed significant $Y_{II}$ levels under natural light in the field (Fig. 3G). Although *C. macrorhizon* is often assumed to be fully mycoheterotrophic (Motomura et al., 2010; Ogura-Tsujita et al., 2012), these results imply that this species indeed performs photosynthetic electron transport in the pericarp under natural conditions. Our data are consistent with the indirect evidence from both stable isotope analysis that has suggested that *C. macrorhizon* fixes significant quantities of carbon at least during the fruiting stage (Suetsugu et al., 2018) and plastome sequence analysis that has shown that plastome of *C. macrorhizon* is almost identical to that of closely related photosynthetic orchids (Kim et al., 2018, 2020). Yuan et al. (2018) reported that the nuclear and plastid genomes of *Gastrodia elata*, an obligate mycoheterotrophic orchid, have lost most genes involved in the photosynthetic electron transport activity, whereas photosynthetic orchids *Phalaenopsis equestris* and *Dendrobium officinale* almost fully retain these photosynthetic genes in their genomes, suggesting a link between the conservation of photosynthetic genes and their nutritional mode. The electron transport activity in *C. macrorhizon* implies that, as are plastid-encoded photosynthetic genes (Kim et al., 2018, 2020), most nuclear-encoded photosynthetic genes would be conserved in this plant. However, several photosynthesis-associated genes are known to cause moderate modifications of photosynthetic properties in *A. thaliana*, which include a fast rise of Chl fluorescence at the photochemical phase of PSII by loss of the *PSBO1* gene (Liu et al., 2007) and increased fluorescence from dissociated antenna complexes by lack of *STN7*-mediated phosphorylation of the light-harvesting complex (LHC) II (Grieco et al., 2015). Therefore, some of genes that are not absolutely necessary for the

236  photosynthetic electron transport may have been lost from the *C. macrorhizon* nuclear

237  genome.

238      Development of stomata are observed on the pericarps of some plants, although the

239  numbers, which greatly differ among plant species, are generally lower compared with

240  those in respective leaves (Simkin et al., 2020). These observations suggest possible

241  contribution of pericarp stomata to gas exchange by fruit, although a role of these stomata

242  in evaporative cooling cannot be ruled out. *C. macrorhizon* is reported to have only

243  degenerated stomata with small stomatal ledges and substomatal chambers on scale

244  leaves of the inflorescence axis (Yukawa and Stern, 2002). We observed development of

245  stomata on the pericarp surfaces of *C. macrorhizon* fruit (Fig. 6B-E). The stomata had no

246  or only underdeveloped substomatal chambers, however, we detected large parenchyma

247  cells containing chloroplasts below the stomata. Considering that *C. macrorhizon* fruit

248  evolves $O_2$ in a light-dependent manner (Fig. 6A), pericarp cells may exchange gases

249  through the degenerated stomata via free diffusion. It should be noted that the density of

250  pericarp stomata in *C. macrorhizon* (17.6 $mm^{-2}$) was lower than those reported in

251  pericarps of *Jatropha curcas* (~70 $mm^{-2}$) (Ranjan et al., 2012) and *Citrus unshiu* (50~300

252  $mm^{-2}$) (Hiratsuka et al., 2015), both of which are shown to perform photosynthetic $CO_2$

253  assimilation in fruits. As suggested in immature green fruit of tomato (*Solanum*

254  *lycopersicum*), which lacks stomata but performs photosynthesis, and other non-foliar

255  tissues of various plants (Simkin et al., 2020), photosynthesis in the *C. macrorhizon*

256  pericarp may function at least partially to re-assimilate $CO_2$ liberated by respiration in

257  mitochondria.

258      Under low light conditions, about 50 $\mu mol\ m^{-2}\ s^{-1}$, the $O_2$-evolving activity of *C.*

259  *macrorhizon* fruit is near the compensation point (Fig. 6A). Therefore, although the fruit

11

260    can perform photosynthetic electron transport, this activity would only partially

261    contribute to net carbon gain. A similar result was reported for *C. trifida*, a leafless orchid

262    with green scales, stems and capsules (Cameron et al., 2009; Zimmer et al., 2008).

263    Although *C. trifida* accumulates Chls and develops active PSII reaction centers, the

264    quantity of carbon fixed by photosynthesis in the field is negligible (Cameron et al., 2009).

265    The marginal carbon fixation in the field and low intrinsic quantum efficiency of PSII in

266    *C. trifida* suggest that the plant is at the late stage in the evolutionary development toward

267    complete mycoheterotrophy (Cameron et al., 2009). The same assumption can be made

268    for *C. macrorhizon*. However, we cannot exclude that Chl accumulation and/or

269    development of photosynthetic machinery in green tissues increases the fitness of this

270    plant. In fact, Suetsugu et al. (2018) suggested that fruiting *C. macrorhizon* plants is not

271    fully mycoheterotrophic, with obtaining ~25% of their total carbon from other than their

272    mycorrhizal fungi. Considering that Chl accumulation is strongly induced during fruiting

273    (Fig. 1) (Suetsugu et al., 2018), photosynthesis in fruit may contribute to mycorrhiza-

274    independent carbon gain for seed production. Based on the $^{13}$C enrichment pattern, Roy

275    et al. (2013) and Gonneau et al. (2014) have shown that photosynthates contribute little

276    to the belowground reserves and emerging shoots that are composed of fungal resources

277    in some Neottieae orchids. In contrast, they also showed that photosynthesis is used for

278    late building of the stem and for fruits production. Moreover, Bellino et al. (2014)

279    reported that a partially mycoheterotrophic orchid *Limodorum abortivum* accumulates

280    Chl in ovaries and employs a compensatory photosynthesis there to buffer fungal carbon

281    limitations and support seed development. It is interesting that a similar trend has been

282    found in other unrelated mixotrophic orchids that have independently evolved partial

283    mycoheterotrophy from *Cymbidium*. Another attractive hypothesis is that Chl

12

284 accumulated in this plant has a certain role other than light energy capture for

285 photosynthesis. In fact, in *A. thaliana*, chlorophyllide produced by dephytylation of Chl

286 in response to cell collapse can suppress the growth of chewing insect herbivores (Hu et

287 al., 2015). Future ecological studies are required to reveal the significance of Chl

288 accumulation (particularly in late stage) and/or photosynthetic electron transport for

289 growth of partially mycoheterotrophic plants including *C. macrorhizon*.

290 　　In contrast to *C. macrorhizon*, *C. goeringii*, which obtains 30% to 50% of its carbon

291 from associated fungi (Motomura et al., 2010), showed high $Y_{II}$ under low actinic light

292 conditions and Fv/Fm comparable to those in *A. thaliana* both in leaves and pericarp (Fig.

293 3A and Fig. S3). Moreover, the photochemical and electron transport capacity of *C.*

294 *goeringii* was similar to that of *A. thaliana* (Fig. S4). The data suggest that *C. goeringii*

295 retains sufficient photosynthetic capacity like fully autotrophic plants at least under low

296 light conditions despite its mixotrophic nutritional mode. Because *C. goeringii* showed

297 higher $Y_{NPQ}$ and lower $Y_{NO}$ in leaves than pericarps particularly under low actinic light

298 (Fig. S3), leaves of this species would have a strong energy dissipation system to protect

299 photosynthetic machinery under low light conditions.

300

301 **Photosynthetic characteristics in green tissues of *C. macrorhizon***

302 Low Fv/Fm in *C. macrorhizon* was mainly attributed to the high Fo level (Fig. 2). Because

303 pericarps of *C. goeringii* and *A. thaliana* showed Fo levels similar to those in respective

304 leaves (Fig. S2), the high Fo is not a common feature of pericarps but specific to *C.*

305 *macrorhizon*. Absorbed light energy that cannot be transferred from the LHCII antenna

306 to the PSII reaction center results in fluorescence emission from the antenna system. Thus,

307 *C. macrorhizon* pericarp may accumulate LHCII antennas that are energetically

308  unconnected with the PSII reaction center. In fact, the thylakoid membrane fraction from

309  *C. macrorhizon* pericarp showed a strong emission peak of Chl fluorescence at ~680 nm

310  at 77K (Fig. 5), which may originate from LHCII dissociated from the PSII core (Krause

311  and Weis, 1991). Because the strong Chl fluorescence at ~680 nm was consistently

312  observed between younger and older fruits of a *C. macrorhizon* plant (Fig. S5), the

313  dissociation of LHCII would not be a result of the maturation or senescence of fruits.

314  Considering that lack of PSII results in high Fo levels (Meurer et al., 1996; Shikanai et

315  al., 1999), functional PSII reaction centers may be few relative to the LHCII antenna in

316  *C. macrorhizon*, which might lead to the high Fo value and low Fv/Fm. Another

317  possibility is that even the short illumination of weak measuring light might reduce $Q_A$

318  and increase the Fo level in *C. macrorhizon*. However, this possibility is unlikely because

319  no increase of Fo by measuring light irradiation, as seen in the constant basal Chl

320  fluorescence before actinic illumination (Fig. 4A,B), was observed in *C. macrorhizon*

321  pericarps as in *A. thaliana* leaves and pericarps.

322     As compared with *A. thaliana*, both *C. goeringii* and *C. macrorhizon* showed strong

323  $Y_{NPQ}$ development with a large $Y_{II}$ reduction in response to increased actinic light, which

324  resulted in the saturation of rETR at lower actinic light intensities (Fig. 3). Together with

325  the low Chl *a*/*b* ratio in *C. goeringii* and *C. macrorhizon* (Table 1), the photosynthetic

326  light-response properties in these orchids may reflect a feature of shade-tolerant plants

327  (Lichtenthaler et al., 1981; Ptushenko et al., 2013). Because shade plants generally show

328  higher proportion of LHCII than LHCI (Lichtenthaler et al., 1981), the high $F_{PSII}/F_{PSI}$ ratio

329  in membrane fractions from *C. macrorhizon* pericarp (Fig. 5) and *C. goeringii* leaves (Fig.

330  S4C) may reflect a higher amount of PSII-LHCII relative to PSI-LHCI. Alternatively, in

331  these orchids, energy spillover from PSII to PSI may be smaller as compared with *A.*

14

332    *thaliana*. In addition to the difference in the $F_{PSI}/F_{PSII}$ ratio, emission peaks of $F_{PSI}$ were

333    red-shifted to ~735 nm in *C. macrorhizon* and *C. goeringii* membranes as compared with

334    that at ~730 nm in *A. thaliana*. Because the association of LHCI to PSI causes red shift

335    of the emission band from the complex at 77K (van Grondelle et al., 1994), the state of

336    the PSI-LHCI association in *C. macrorhizon* and *C. goeringii* may differ from that in *A.*

337    *thaliana*.

338    Of note, *C. macrorhizon* pericarp showed substantially high $F_{PSII}/F_{PSI}$ ratio even

339    compared with *C. goeringii* leaves. Our data suggest that *C. macrorhizon* has LHCII

340    energetically disconnected from the PSII reaction center, which may emit strong

341    fluorescence at 77K as shown in previous studies (Haferkamp et al., 2010; Rantala et al.,

342    2017). As discussed earlier, the accumulation of LHCII free from the functional reaction

343    center may also explain the high Fo level in *C. macrorhizon*. In addition, the Chl *a*/*b* ratio

344    was notably low in *C. macrorhizon* even compared with *C. goeringii* (Table 1), which

345    also implies unique antenna-reaction center compositions in this plant. Similarly, the low

346    Chl *a*/*b* ratio around 2 or below was observed in *L. abortivum*, *C. trifida*, and

347    *Cephalanthera damasonium*, which are also partially mycoheterotrophic orchids (Bellino

348    et al., 2014; Cameron et al., 2009; Zimmer et al., 2008). Thus, there may be physiological

349    and ecological implications of the low Chl *a*/*b* ratio common to these partially

350    mycoheterotrophic orchids.

351    Polyphasic increases of Chl fluorescence in a logarithmic time series with

352    illumination (Fig. 4A) is explained by a stepwise retardation of the photosynthetic

353    electron flow from primary photochemical reactions in PSII to later reduction processes

354    at the acceptor side of PSI (Krause and Weis, 1991). Unlike *A. thaliana* leaves and

355    pericarp, *C. macrorhizon* pericarp showed immediate induction of Chl fluorescence with

15

illumination (Fig. 4A), which indicates limited electron transport capacity of the PSII

reaction center. It is noteworthy that, in *C. macrorhizon* pericarp, the $Q_A$ reoxidation in

PSII after a single saturation flash was as fast as in *A. thaliana* leaves (Fig. 4B). Therefore,

the electron transport at the acceptor side of PSII is functional in *C. macrorhizon*. The

oxidized plastoquinone pools in *C. macrorhizon* pericarp particularly under low light,

which were represented by the qP level comparable to those in *A. thaliana* and *C.

goeringii* (Fig. 3E), also implicate effective electron transport downstream of PSII in this

plant tissue. Meanwhile, Fv'/Fm' was notably low in *C. macrorhizon* pericarp (Fig. 3D),

which suggest that the low $Y_{II}$ in *C. macrorhizon* pericarp mainly results from the low

quantum efficiency of PSII photochemistry.

In this study, we revealed some notable features of photosynthetic properties in *C.

macrorhizon*, which includes the substantially low Chl *a/b* ratio and Fv/Fm (Table 1),

very fast Chl fluorescence induction with illumination (Fig. 4A), and the high $F_{PSII}/F_{PSI}$

ratio and blue shift of $F_{PSII}$ at 77 K (Fig. 5). Nonetheless, the *C. macrorhizon* shoot

retained the photosynthetic electron transport activity not only under laboratory

conditions (Fig. 3A) but also in the field (Fig. 3G). Moreover, this species showed light-

dependent development of nonphotochemical quenching (Fig. 3B), fast $Q_A$ reoxidation

activity in PSII (Fig. 4B), photosystem complex formation (Fig. 5), and light-dependent

$O_2$ evolution (Fig. 6A). These data demonstrate that *C. macrorhizon* retains most of major

photosynthetic components in chloroplasts, consistent with the highly conserved

plastome structure (Kim et al., 2018, 2020) and the partial autotrophic activity (Suetsugu

et al., 2018) in this species. Despite ample plastid genome data from various leafless

orchids (e.g. Kim et al., 2018, 2020), the actual degeneration processes of photosynthetic

function during heterotrophic evolution remain unclear. Our detailed characterization of

16

380  the photosynthetic machinery in leafless *C. macrorhizon* shed light on diverse mode of

381  photosynthesis and its regulation depending on life histories of partially heterotrophic

382  plants. Our data provide the insight into the degenerate process of photosynthesis during

383  mycoheterotrophic evolution.

384

385  *Materials and Methods*

386  **Plant materials**

387  *C. macrorhizon* samples with immature and mature fruits were collected in December

388  2015 and October 2016 from an evergreen forest dominated by *Quercus glauca* in

389  Tsuzuki-ku, Yokohama, Japan (35°33′N and 139°34′E). Samples were kept in the

390  laboratory under a fluorescent light (~20 μmol photons $m^{-2}$ $s^{-1}$) at room temperature

391  (23~25°C) for several hours to 1 day before experiments with their roots wrapped with

392  wet paper. *C. goeringii* samples collected in December 2015 and October 2016 from a

393  wooded area in Sanbu-City, Chiba, Japan (35°38′N, 140°22′E) were grown on soil under

394  laboratory conditions with natural light (~100 μmol photons $m^{-2}$ $s^{-1}$). To analyze fruits, *C.*

395  *goeringii* flowers were hand-pollinated in March, and fruits matured in June were used

396  for experiments. *A. thaliana* Columbia ecotype was grown on agar-solidified Murashige

397  and Skoog medium (adjusted to pH 5.7 with KOH) containing 1% (w/v) sucrose at 23°C

398  in a growth chamber (~100 μmol photons $m^{-2}$ $s^{-1}$).

399

400  **Pigment determination**

401  For pigment determination, pericarp (~2 mm thick) from *C. macrorhizon* and *C. goeringii*

402  was cut off from whole fruit by using a fine razor and *C. macrorhizon* stem of ~2 cm

403  length was cut at 3 cm from the stem-root junction. For comparison, pigments were

404     extracted from ~1 cm segments of healthy *C. goeringii* leaves, the third or fourth true

405     leaves of 21-d-old *A. thaliana* seedlings, and *A. thaliana* pericarps from mature siliques

406     of 5 to 7-week-old plants. Plant samples were crushed in liquid nitrogen and mixed with

407     80% (v/v) acetone to extract hydrophobic pigments. Cell debris was removed from the

408     extract by centrifugation at $10,000 \times g$ for 5 min. Absorption spectra of the supernatant

409     were measured every 0.2 nm from 400 to 750 nm wavelength. Obtained spectra were

410     normalized at the peak, 664 nm, as 1 and the background absorption, 750 nm, as 0. To

411     determine Chl and carotenoid contents, the absorbance of the supernatant at 720, 663.2,

412     646.8, 645 and 470 nm was measured by using a V-730 BIO spectrophotometer (JASCO;

413     Japan) as described in Melis *et al*. (1987) and Lichtenthaler (1987). The Chl *a*/*b* ratio in

414     *C. macrorhizon* pericarps and *A. thaliana* leaves and pericarps was also confirmed by the

415     equations of Porra et al., (1989) (Fig. S1).

416

**Pulse amplitude modulation (PAM) analysis of Chl fluorescence**

417

418     Chl fluorescence parameters in laboratory conditions were analyzed by using an imaging

419     PAM fluorometer (IMAGING-PAM MAXI, Walz, Germany) and ImagingWin software.

420     Samples incubated under dim light (~5 μmol photons $m^{-2}$ $s^{-1}$) for ~1 h were dark-treated

421     for 15 min in the device. After determination of Fo with the lowest measuring light

422     intensity (~0.2 μmol photon $m^{-2}$ $s^{-1}$ at a frequency of 2 Hz), samples were illuminated

423     with a saturating pulse flash (~3400 μmol photon $m^{-2}$ $s^{-1}$ for 720 ms) to determine

424     maximal Chl fluorescence (Fm). Then samples were illuminated with actinic light of

425     given intensity for 3 min and second saturating pulse to determine stationary (F) and

426     maximal fluorescence under light (Fm'), respectively. Photosynthetic photon flux density

427     (PPFD) of actinic light was successively increased every 3 min to 10, 20, 35, 80, 145,

428    280, 395 and 610 μmol photons $m^{-2}$ $s^{-1}$. Minimal fluorescence after actinic illumination

429    (Fo') was computed by the approximation of Oxborough and Baker (1997). These

430    fluorescence yields were used to calculate Fv/Fm, $Y_{II}$, $Y_{NPQ}$ and $Y_{NO}$, qP, and Fv'/Fm'

431    (Kramer et al., 2004; Maxwell and Johnson, 2000). We also computed $Y_{II}$, $Y_{NPQ}$ and $Y_{NO}$

432    ($Y_C$) according to Guandagno et al. (2010), which does not require Fo' for calculation,

433    and confirmed no noticeable difference of the values from those according to Kramer et

434    al., (2004). rETR was determined by multiplying $Y_{II}$ with PPFD.

435    For $Y_{II}$ measurement of *C. macrorhizon* pericarp in the field, F and Fm' of mature *C.*

436    *macrorhizon* fruit grown at Tsuzuki-ku, Yokohama, Japan, were determined with a fiber

437    optic PAM fluorometer under sunlight (Junior-PAM, Walz) at ~21°C and ~53% humidity

438    on October 14, 2016. Measuring light of ~0.02 μmol photons $m^{-2}$ $s^{-1}$ at a frequency of 10

439    Hz and saturation pulse of ~5800 μmol photons $m^{-2}$ $s^{-1}$ for 500 ms were used in the Junior-

440    PAM analysis. PPFD of natural light was measured with a light meter (Li-190SA and LI-

441    250A, LI-COR) placed beside samples.

442

443    **Measurement of fast-induction and decay kinetics of Chl fluorescence from PSII**

444    All samples were incubated under low light (~5 μmol photons $m^{-2}$ $s^{-1}$) for ~30 min and

445    then in the dark for 5 min before experiments. Fast-induction and decay kinetics of Chl

446    fluorescence was determined by measuring Chl fluorescence directly from fresh samples

447    in a quartz cuvette under 2 μmol photons $m^{-2}$ $s^{-1}$ measuring light with a FL-3500

448    fluorometer (Photon Systems Instruments). Data were collected in a logarithmic time

449    series between 0.2 ms and 5 s after the onset of actinic light of 400 μmol photons $m^{-2}$ $s^{-1}$.

450    Decay kinetics of Chl fluorescence after a single saturation flash was measured between

451    0.2 ms and 60 s with FL3500. Fluorescence transients of the induction and decay analyses

452  were normalized between minimal and maximal Chl fluorescence to range from 0 to 1.

453

**Chl fluorescence analysis in thylakoid membrane fractions at 77K**

455  To prepare thylakoid membrane fractions, samples were pulverized in liquid nitrogen and

456  homogenized in a cold buffer (0.33 M sorbitol, 5 mM MgCl2, 5 mM EDTA, 50 mM

457  HEPES-KOH, pH 7.6). The homogenate was filtered through a single layer of Miracloth

458  (Calbiochem) with gentle hand pressure. After centrifugation at 5,000 g for 10 min at 4°C,

459  the supernatant was discarded, and the pellet was resuspended in a cold buffer to obtain

460  1 μg/ml Chl-containing membrane fractions. Chl fluorescence spectra of the membrane

461  fractions from 620 to 800 nm were measured in liquid nitrogen by use of an RF-5300PC

462  spectrofluorometer (Shimadzu) under 435-nm excitation. Chl fluorescence emission data

463  were normalized to the mean value between 650nm and 800 nm after subtracting the value

464  at 800 nm as background.

465

**Measurement of $O_2$-evolving activity of C. macrorhizon fruit**

467  Intact *C. macrorhizon* fruit was placed in a cylinder-type $O_2$ electrode chamber (DW1/AD,

468  Hansatech) of closed air conditions with the atmospheric $CO_2$ concentration, and $O_2$

469  evolution rate was measured with a Clark-type $O_2$ electrode (Oxygraph Plus, Hansatech)

470  at 23°C under 470 nm-monochromatic blue light (ISL-mini, CCS). Light intensity was

471  increased from 0 to 400 μmol photons $m^{-2}$ $s^{-1}$ every 3 min during the measurement.

472

**Microscopic analysis of stomata**

474  Surface structures of *C. macrorhizon* pericarp were observed by SEM (VE-8800,

475  Keyence) at 10 kV. Stomatal density was determined by counting the number of stomata

20

476　in 1.13 mm$^2$ in SEM images. To analyze longitudinal sections of *C. macrorhizon* pericarp,

477　fresh pericarp tissues were cut into ~50-μm sections by using a plant microtome (MTH-

478　1, NK system). The sections were observed under a light microscope (BX50, Olympus).

479

483

486

489

490　***References***

491　Bellino, A., Alfani, A., Selosse, M.A., Guerrieri, R., Borghetti, M., and Baldantoni, D.

492　　(2014) Nutritional regulation in mixotrophic plants: New insights from *Limodorum*

493　　*abortivum*. *Oecologia*. 175: 875–885.

494　Cameron, D.D., Preiss, K., Gebauer, G., and Read, D.J. (2009) The chlorophyll-

495　　containing orchid *Corallorhiza trifida* derives little carbon through photosynthesis.

496　　*New Phytol*. 183: 358–364.

497　Gebauer, G., and Meyer, M. (2003) $^{15}$N and $^{13}$C natural abundance of autotrophic and

498　　myco-heterotrophic orchids provides insight into nitrogen and carbon gain from

499　　fungal association. *New Phytol*. 160: 209–223.

500    Grieco, M., Suorsa, M., Jajoo, A., Tikkanen, M., and Aro, E.M. (2015) Light-harvesting

501        II antenna trimers connect energetically the entire photosynthetic machinery -

502        Including both photosystems II and I. *Biochim Biophys Acta.* 1847: 607–619.

503    van Grondelle, R., Dekker, J.P., Gillbro, T., and Sundstrom, V. (1994) Energy transfer

504        and trapping in photosynthesis. *Biochim Biophys Acta*. 1187: 1–65.

505    Gonneau, C., J. Jersáková, E. de Tredern, I. Till‑Bottraud, K. Saarinen, M. Sauve, M.

506        Roy, et al. 2014. Photosynthesis in perennial mixotrophic *Epipactis* spp.

507        (Orchidaceae) contributes more to shoot and fruit biomass than to hypogeous

508        survival. *Journal of Ecology* **102**: 1183– 1194.

509    Guadagno, C.R., Virzo De Santo, A., and D'Ambrosio, N. (2010) A revised energy

510        partitioning approach to assess the yields of non-photochemical quenching

511        components. *Biochim Biophys Acta*. 1797: 525–530.

512    Haferkamp, S., Haase, W., Pascal, A.A., Van Amerongen, H., and Kirchhoff, H. (2010)

513        Efficient light harvesting by photosystem II requires an optimized protein packing

514        density in grana thylakoids. *J Biol Chem*. 285: 17020–17028.

515    Hiratsuka, S., Suzuki, M., Nishimura, H., and Nada, K. (2015) Fruit photosynthesis in

516        Satsuma mandarin. *Plant Sci.* 241: 65–69.

517    Hu, X., Makita, S., Schelbert, S., Sano, S., Ochiai, M., Tsuchiya, T., et al. (2015)

518        Reexamination of chlorophyllase function implies its involvement in defense

519        against chewing herbivores. *Plant Physiol*. 167: 660–670.

520    Kim, H.T., Shin, C.H., Sun, H., and Kim, J.H. (2018) Sequencing of the plastome in the

521        leafless green mycoheterotroph *Cymbidium macrorhizon* helps us to understand an

522        early stage of fully mycoheterotrophic plastome structure. *Plant Syst Evol*. 304:

523        245–258.

524     Kim, Y.K., Jo, S., Cheon, S.H., Joo, M.J., Hong, J.R., Kwak, M., et al. (2020) Plastome

525          evolution and phylogeny of Orchidaceae, with 24 new sequences. *Front Plant Sci*.

526          11: 22.

527     Kramer, D.M., Johnson, G., Kiirats, O., and Edwards, G.E. (2004) New fluorescence

528          parameters for the determination of $Q_A$ redox state and excitation energy fluxes.

529          *Photosynth Res*. 79: 209–218.

530     Krause, G.H., and Weis, E. (1991) Chlorophyll fluorescence and photosynthesis: the

531          basics. *Annu Rev Plant Physiol Plant Mol Biol*. 42: 313–349.

532     Leake, J.R. (1994) The biology of myco-heterotrophic ('saprophytic') plants. *New*

533          *Phytol*. 127: 171–216.

534     Lichtenthaler, H.K. (1987) Chlorophylls and carotenoids: Pigments of photosynthetic

535          biomembranes. *Methods Enzymol*. 148: 350–382.

536     Lichtenthaler, H.K., Buschmann, C., Döll, M., Fietz, H.J., Bach, T., Kozel, U., et al.

537          (1981) Photosynthetic activity, chloroplast ultrastructure, and leaf characteristics of

538          high-light and low-light plants and of sun and shade leaves. *Photosynth Res*. 2:

539          115–141.

540     Liu, H., Frankel, L.K., and Bricker, T.M. (2007) Functional analysis of photosystem II

541          in a PsbO-1-deficient mutant in *Arabidopsis thaliana*. *Biochemistry*. 46: 7607–

542          7613.

543     Maxwell, K., and Johnson, G.N. (2000) Chlorophyll fluorescence--a practical guide. *J*

544          *Exp Bot*. 51: 659–668.

545     Melis, A., Spangfort, M., and Andersson, B. (1987) Light-absorption and electron

546          transport balance between photosystem II and photosystem I in spinach

547          chloroplasts. *Photochem Photobiol*. 45: 129–136.

548    Meurer, J., Meierhoff, K., and Westhoff, P. (1996) Isolation of high-chlorophyll-

549        fluorescence mutants of *Arabidopsis thaliana* and their characterisation by

550        spectroscopy, immunoblotting and Northern hybridisation. *Planta*. 49: 385–396.

551    Montfort, C., and Küsters, E. (1940) Saprophytismus und Photosynthese. I.

552        Biochemische und physiologische Studien an Humus-Orchideen. *Bot Arch*. 40:

553        571–633.

554    Motomura, H., Selosse, M.-A., Martos, F., Kagawa, A., and Yukawa, T. (2010)

555        Mycoheterotrophy evolved from mixotrophic ancestors: Evidence in *Cymbidium*

556        (Orchidaceae). *Ann Bot*. 106: 573–581.

557    Ogura-Tsujita, Y., Yokoyama, J., Miyoshi, K., and Yukawa, T. (2012) Shifts in

558        mycorrhizal fungi during the evolution of autotrophy to mycoheterotrophy in

559        *Cymbidium* (Orchidaceae). *Am J Bot*. 99: 1158–1176.

560    Oxborough, K., and Baker, N.R. (1997) Resolving chlorophyll a fluorescence images of

561        photosynthetic efficiency into photochemical and non-photochemical components

562        – calculation of qP and Fv'/Fm' without measuring Fo'. *Photosynth Res*. 54: 135–

563        142.

564    Porra, R.J., Thompson, W.A., and Kriedemann, P.E. (1989) Determination of accurate

565        extinction coefficients and simultaneous equations for assaying chlorophylls *a* and

566        *b* extracted with four different solvents: verification of the concentration of

567        chlorophyll standards by atomic absorption spectroscopy. *Biochim Biophys Acta*.

568        975: 384–394.

569    Ptushenko, V. V., Ptushenko, E.A., Samoilova, O.P., and Tikhonov, A.N. (2013)

570        Chlorophyll fluorescence in the leaves of Tradescantia species of different

571        ecological groups: Induction events at different intensities of actinic light.

572     *BioSystems*. 114: 85–97.

573     Ranjan, S., Singh, R., Soni, D.K., Pathre, U. V., and Shirke, P.A. (2012) Photosynthetic

574         performance of *Jatropha curcas* fruits. *Plant Physiol Biochem.* 52: 66–76.

575     Rantala, M., Tikkanen, M., and Aro, E.M. (2017) Proteomic characterization of

576         hierarchical megacomplex formation in Arabidopsis thylakoid membrane. *Plant J.*

577         92: 951–962.

578     Roy, M., C. Gonneau, A. Rocheteau, D. Berveiller, J. C. Thomas, C. Damesin, and M.

579         A. Selosse. 2013. Why do mixotrophic plants stay green? A comparison between

580         green and achlorophyllous orchid individuals in situ. *Ecological*

581         *Monographs* **83**: 95– 117.

582     Selosse, M.A., and Roy, M. (2009) Green plants that feed on fungi: facts and questions

583         about mixotrophy. *Trends Plant Sci.* 14: 64–70.

584     Shikanai, T., Munekage, Y., Shimizu, K., Endo, T., and Hashimoto, T. (1999)

585         Identification and characterization of *Arabidopsis* mutants with reduced quenching

586         of chlorophyll fluorescence. *Plant Cell Physiol*. 40: 1134–1142.

587     Simkin, A.J., Faralli, M., Ramamoorthy, S., and Lawson, T. (2020) Photosynthesis in

588         non-foliar tissues: implications for yield. *Plant J.* 101: 1001–1015.

589     Suetsugu, K., Ohta, T., and Tayasu, I. (2018) Partial mycoheterotrophy in the leafless

590         orchid *Cymbidium macrorhizon*. *Am J Bot*. 105: 1595–1600.

591     Yuan, Y., Jin, X., Liu, J., Zhao, X., Zhou, J., Wang, X., et al. (2018) The *Gastrodia*

592         *elata* genome provides insights into plant adaptation to heterotrophy. *Nat Commun.*

593         9: 1615.

594     Yukawa, T., and Stern, W.L. (2002) Comparative vegetative anatomy and systematics

595         of *Cymbidium* (Cymbidieae: Orchidaceae). *Bot J Linn Soc*. 138: 383–419.

596    Zimmer, K., Meyer, C., and Gebauer, G. (2008) The ectomycorrhizal specialist orchid

597        *Corallorhiza trifida* is a partial myco-heterotroph. *New Phytol.* 178: 395–400.

598

**Table 1.** Pigment composition and maximum photosynthetic quantum yield (Fv/Fm) of *C. macrorhizon*, *C. goeringii* and *A. thaliana*.

| Plant materials | | Chl *a* | Chl *b* | Car | Chl *a/b* | Chl *a*/Car | Fv/Fm |
|---|---|---|---|---|---|---|---|
| | | nmol g$^{-1}$ FW | nmol g$^{-1}$ FW | µg g$^{-1}$ FW | mol/mol | nmol/µg | |
| *A. thaliana* | leaf | 2331.6±28.3 | 751.3±9.8 | 472.7±14.4 | 3.10±0.00 | 4.94±0.15 | 0.79±0.00 |
| | pericarp | 1035.5±68.7 | 302.0±20.5 | 204.3±12.2 | 3.43±0.03 | 5.07±0.07 | 0.77±0.00 |
| *C. goeringii* | leaf | 2496.7±75.4 | 867.9±43.0 | 554.7±24.4 | 2.89±0.07 | 4.51±0.16 | 0.79±0.00 |
| | pericarp | 167.4±9.9 | 77.4±7.2 | 34.3±3.1 | 2.18±0.08 | 4.91±0.16 | 0.75±0.01 |
| *C. macrorhizon* | stem | 50.0±5.9 | 30.7±3.4 | 18.2±3.2 | 1.63±0.03 | 2.83±0.23 | 0.57±0.03 |
| | pericarp | 96.0±13.9 | 53.3±7.6 | 29.1±4.2 | 1.80±0.01 | 3.35±0.21 | 0.57±0.02 |

Data are mean ± SE (n = 3). Car, carotenoids.

599

600

601

602 **Fig. 1** *C. macrorhizon* growing in an evergreen forest dominated by *Quercus glauca* in

603 Yokohama, Japan. Pale green pericarp at the flowering stage showed stronger green color

604 during fruit maturation. The approximate length of mature *C. macrorhizon* fruits was 3

605 cm.

606
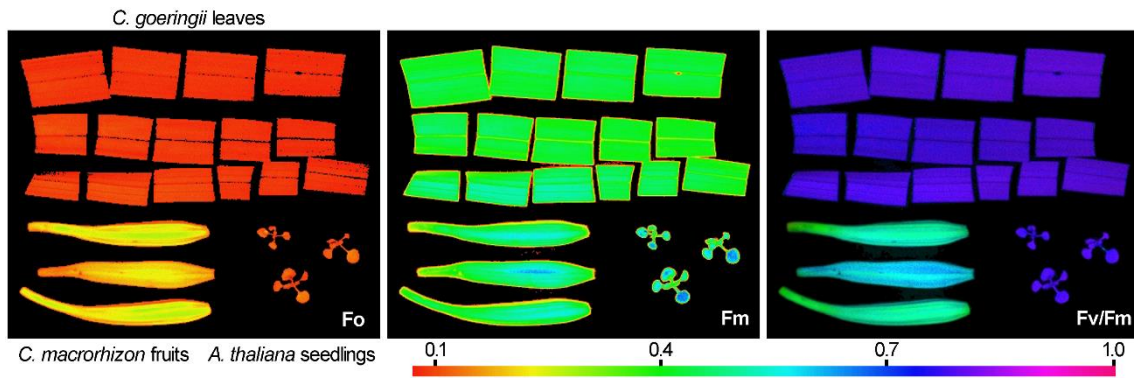
607

608 **Fig. 2** Chl fluorescence images of *C. macrorhizon* fruits, *C. goeringii* leaves and *A.*

609 *thaliana* seedlings. *C. goeringii* leaves were cut into rectangles to avoid curling during

610 the analysis. Left, middle and right panels show images of minimum fluorescence (Fo),

611 maximum fluorescence (Fm), and maximum quantum yield of PSII (Fv/Fm), respectively.

612 The color represents the value of each parameter in the color scale from red (0.075) to

613 purple (1.0).

614
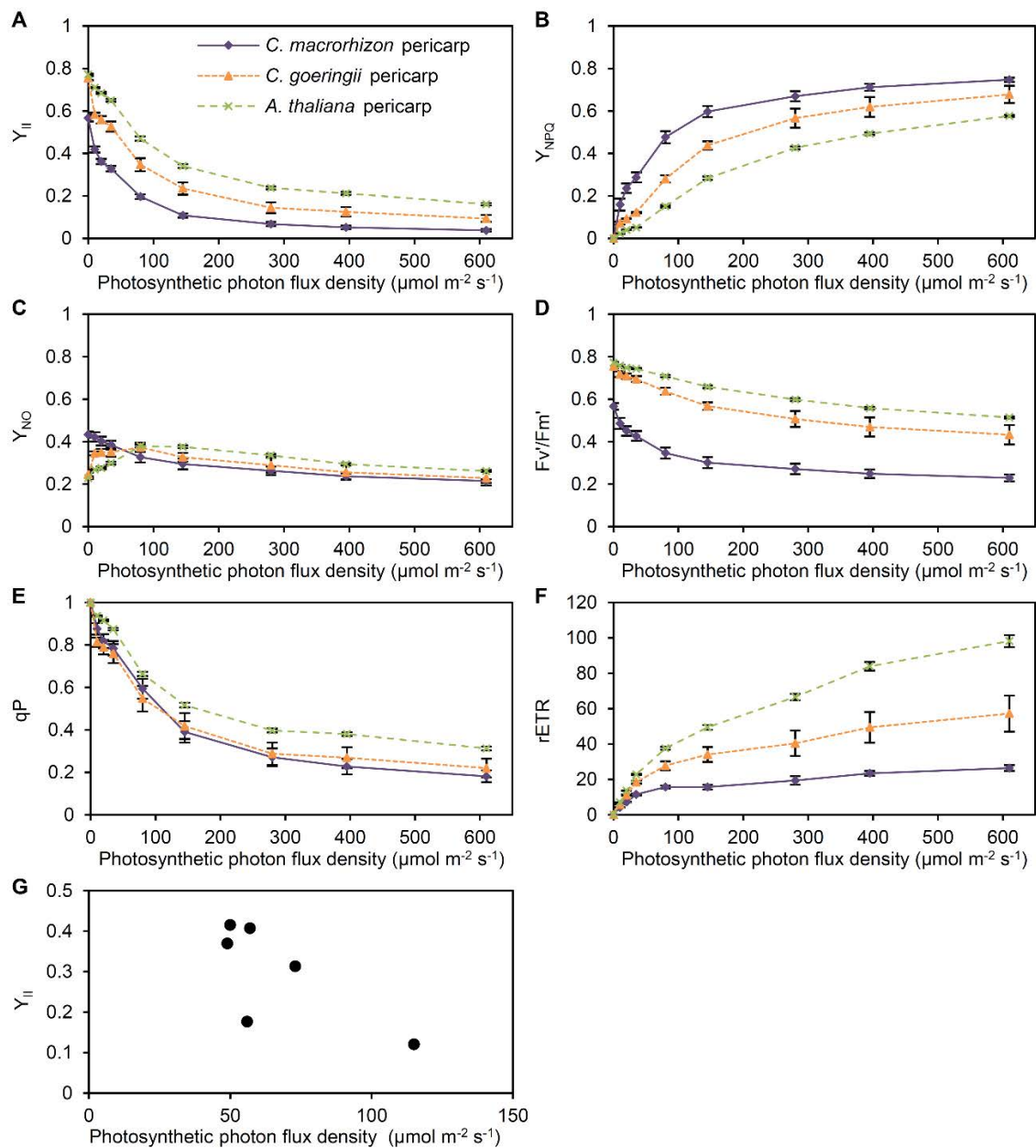
**Fig. 3** Light-response curves of quantum yields of (A) photosystem II ($Y_{II}$), (B) regulated thermal energy dissipation ($Y_{NPQ}$) and (C) non-regulated energy dissipation ($Y_{NO}$), (D) Maximum PSII quantum yield under actinic light conditions (Fv'/Fm'), (E) Coefficient of photochemical quenching (qP), and (F) relative electron transport rate (rETR) in pericarps of *C. macrorhizon*, *C. goeringii* and *A. thaliana*. Data are mean ± SE (n = 12). (G) $Y_{II}$ of *C. macrorhizon* pericarp under natural light conditions in an evergreen forest in Yokohama, Japan. Six different individuals were examined.

30

623



624
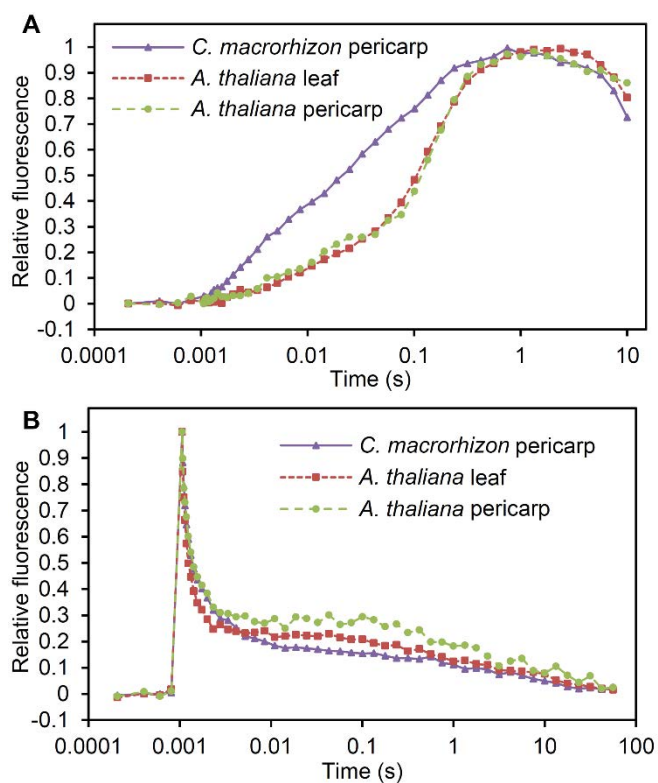
**Fig. 4** Fast induction (A) and decay kinetics (B) of Chl fluorescence in *C. macrorhizon* pericarps and leaves and pericarps of *A. thaliana*. Data are means from 3 independent tissue samples.

628

31

629
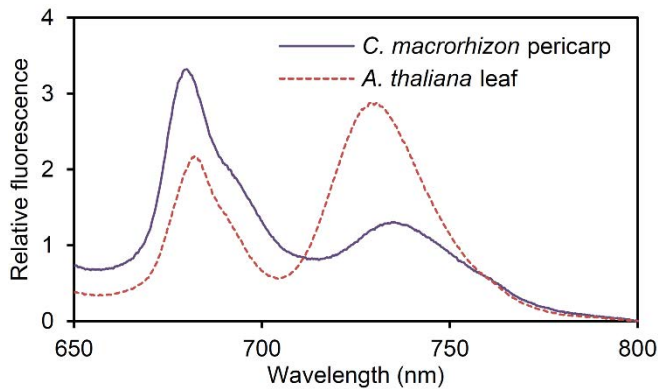


630

631   **Fig. 5** Emission spectra of Chl fluorescence at 77K in the thylakoid membrane fraction

632   from *C. macrorhizon* pericarps and *A. thaliana* leaves. Each spectrum was normalized to

633   the mean value between 650 nm and 800 nm with background correction at 800 nm. Data

634   are means from 6 independent tissue samples for both plants. The mean peak wavelength

635   of Chl fluorescence from PSII ($F_{PSII}$) is 680.0 nm (SD = 0.9 nm) for *C. macrorhizon*

636   pericarps and 682.3 nm (SD = 0.2 nm) for *A. thaliana* leaves, and that from PSI ($F_{PSI}$) is

637   735.2 nm (SD = 0.6 nm) for *C. macrorhizon* pericarps and 729.6 nm (SD = 0.7 nm) for

638   *A. thaliana* leaves. The mean $F_{PSII}/F_{PSI}$ ratio is 2.59 (SD = 0.54) for *C. macrorhizon*

639   pericarps and 0.75 (SD = 0.69) for *A. thaliana* leaves.

640

641
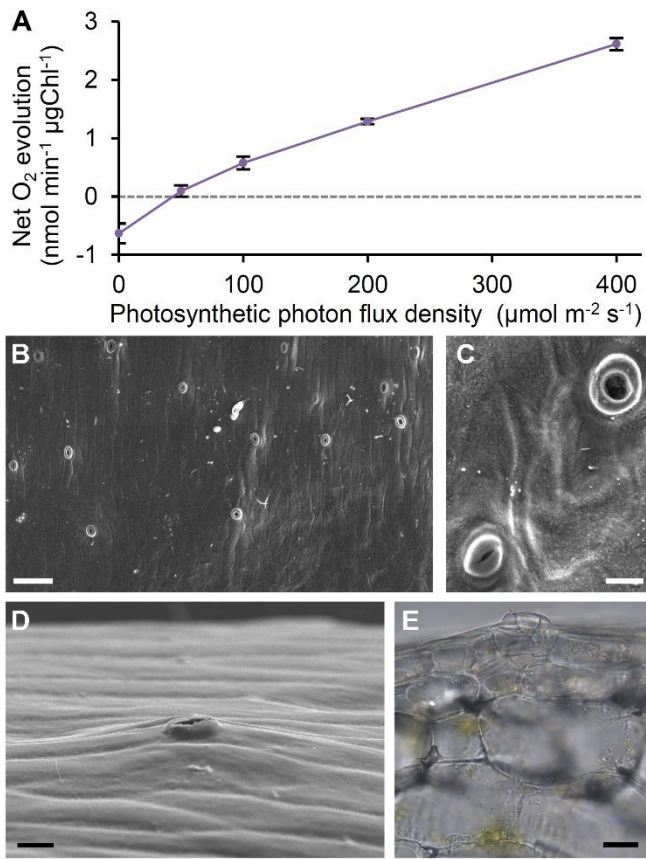
**Fig. 6** (A) Light-response curve of net $O_2$-evolving activity in intact fruit of *C. macrorhizon*. Data are mean ± SE from 3 independent tissue samples. (B-D) Scanning electron micrographs of *C. macrorhizon* pericarp. (E) A longitudinal section of *C. macrorhizon* pericarp observed under a light microscope. Arrowhead indicates a stoma on the pericarp surface. Bars = 100 μm in (B) and 20 μm in (C-E).

647

648 *Supplementary Data*



649
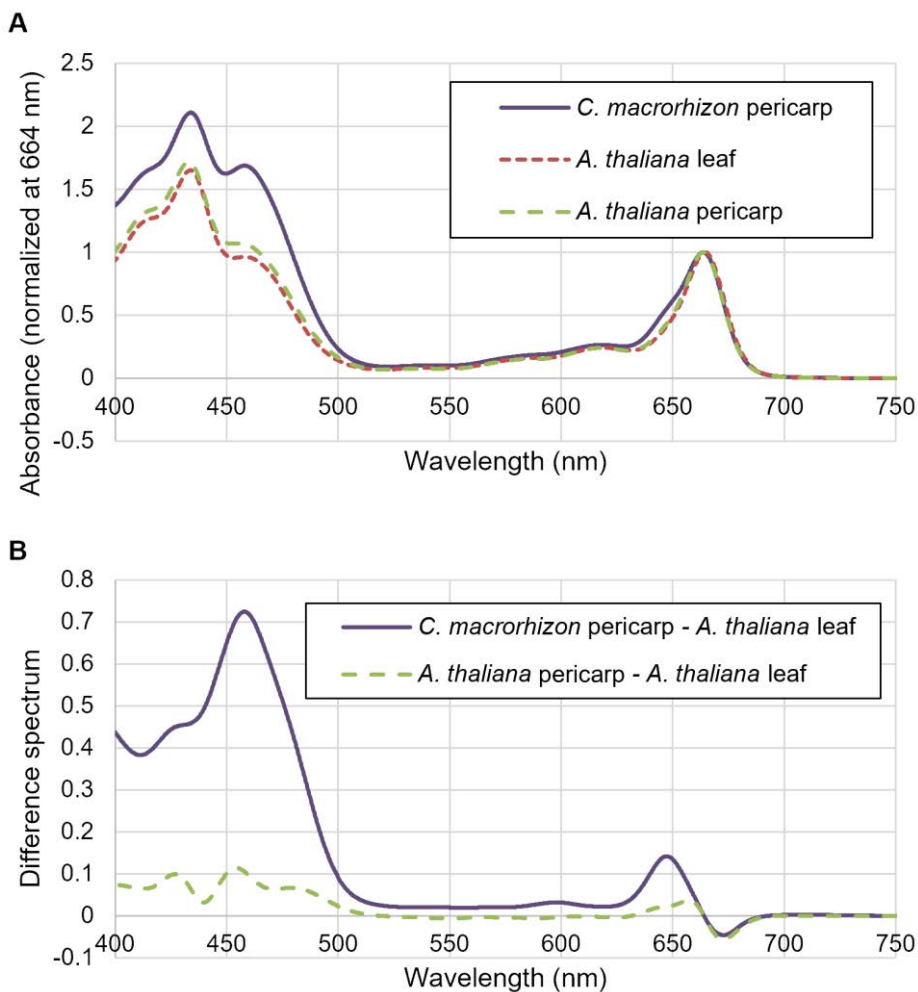
**Fig. S1** Absorption spectra of pigments extracted from pericarp of *C. macrorhizon* were compared with those from leaves and pericarp of *A. thaliana*. (A) The spectra were normalized at the peak, 664 nm, as 1 and the background absorption, 750 nm, as 0. The Chl *a/b* ratio according to Porra et al. (1989) was 1.84 (SD = 0.06, n = 6) for *C. macrorhizon* pericarps, 3.60 (SD = 0.05, n = 3) for *A. thaliana* leaves, and 3.17 (SD = 0.04, n = 3) for *A. thaliana* pericarps. (B) Differences of the normalized spectra between *C. macrorhizon* pericarp or *A. thaliana* pericarp and *A. thaliana* leaves.

657
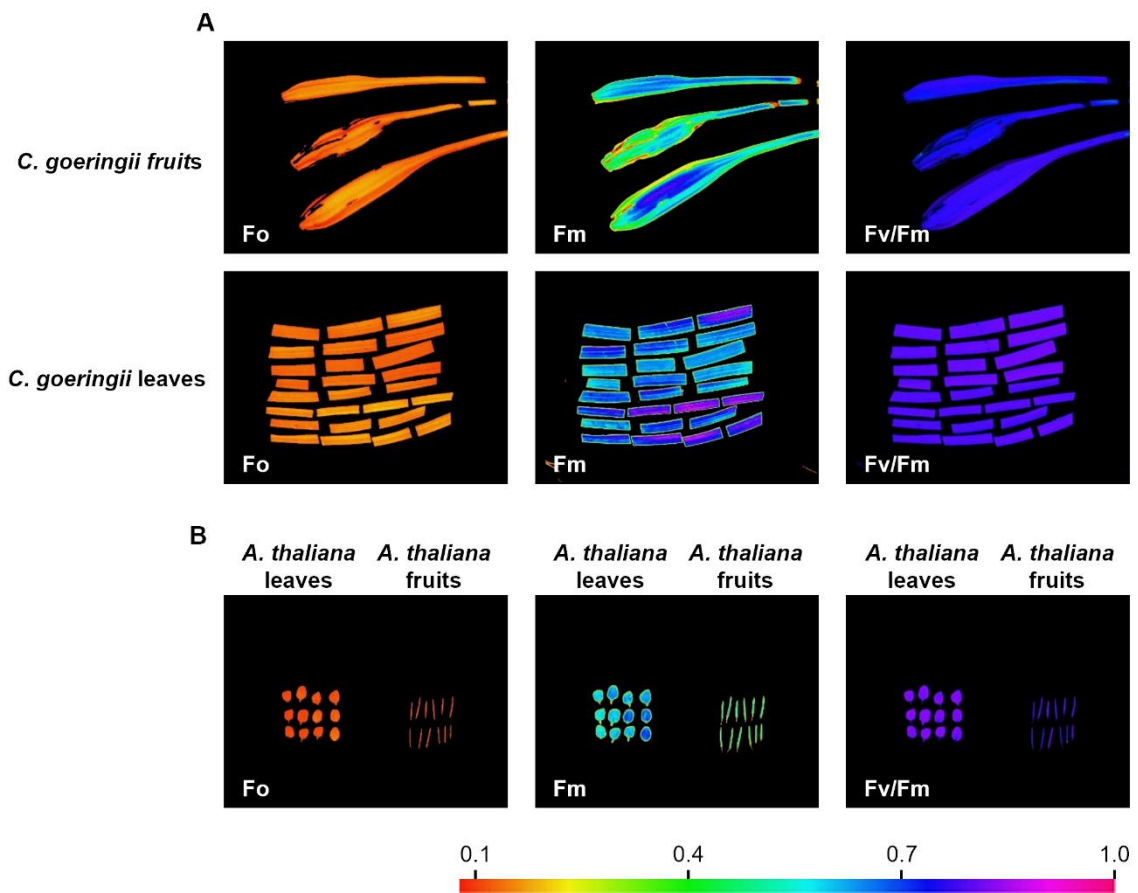
**Fig. S2** Chl fluorescence images of fruits and leaves of (A) *C. goeringii* and (B) *A. thaliana*. *C. goeringii* leaves were cut into rectangles to avoid curling during the analysis. Left, middle and right panels show images of minimum fluorescence (Fo), maximum fluorescence (Fm), and maximum quantum yield of PSII (Fv/Fm), respectively. The color represents the value of each parameter in the color scale from red (0.075) to purple (1.0).
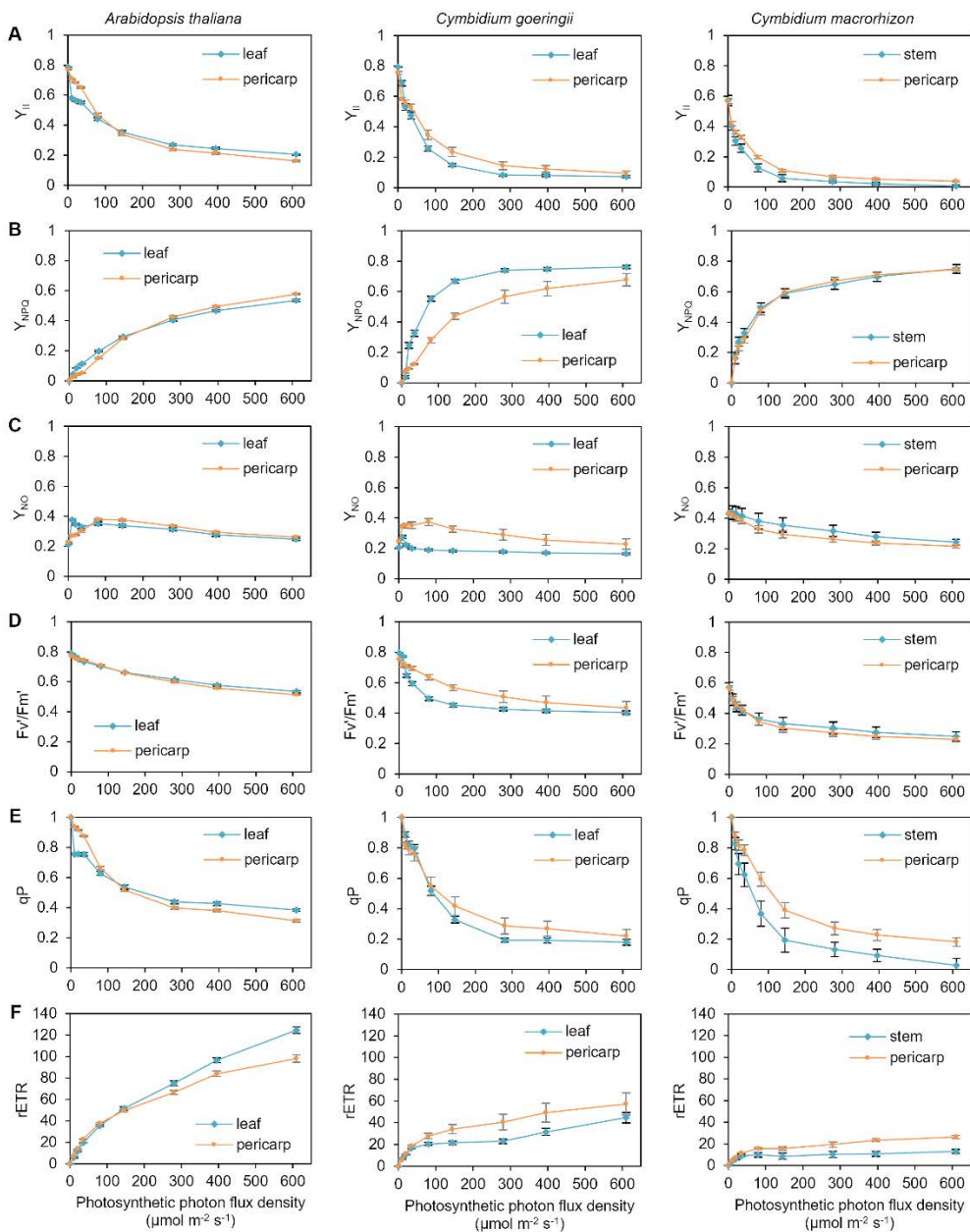
666

667  **Fig. S3** Light-response curves of quantum yields of (A) photosystem II ($Y_{II}$), (B)

668  regulated thermal energy dissipation ($Y_{NPQ}$) and (C) non-regulated energy dissipation

669  ($Y_{NO}$), (D) Maximum PSII quantum yield under actinic light conditions (Fv'/Fm'), (E)

670  Coefficient of photochemical quenching (qP), and (F) relative electron transport rate

671  (rETR) are compared between two different tissues in *A. thaliana* (leaf and pericarp), *C.*

672  *goeringii* (leaf and pericarp) and *C. macrorhizon* (stem and pericarp). Data are mean ±

673  SE from n>5 independent tissue samples.
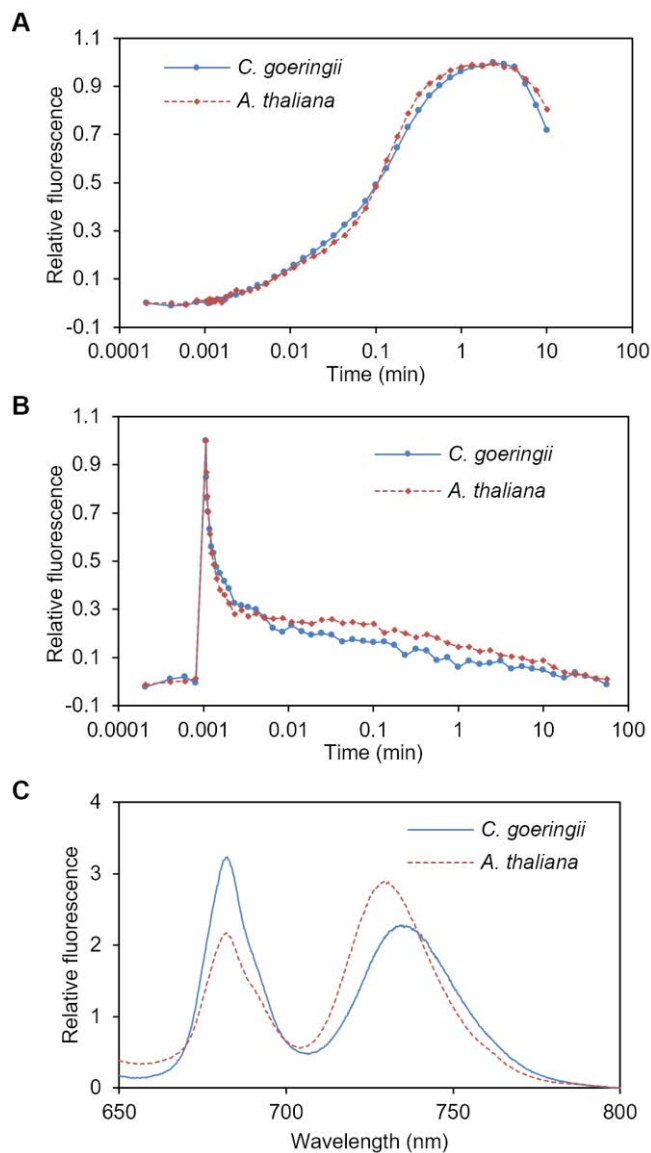
**Fig. S4** Fast induction (A) and decay kinetics (B) of Chl fluorescence in *C. goeringii* leaves (n = 6). (C) Emission spectra of Chl fluorescence at 77K in the thylakoid membrane fraction from *C. goeringii* leaves (n = 3). The mean peak wavelength of Chl fluorescence from PSII ($F_{PSII}$) is 682.1 nm (SD = 0.3 nm) and that from PSI ($F_{PSI}$) is 735.0 nm (SD = 1.1 nm). The mean $F_{PSII}/F_{PSI}$ ratio is 1.41 (SD = 0.09). The spectrum was normalized to the mean value between 650 nm and 800 nm with background correction at 800 nm. Data in *A. thaliana* (Figs. 4 and 5) were shown together as comparison.

37
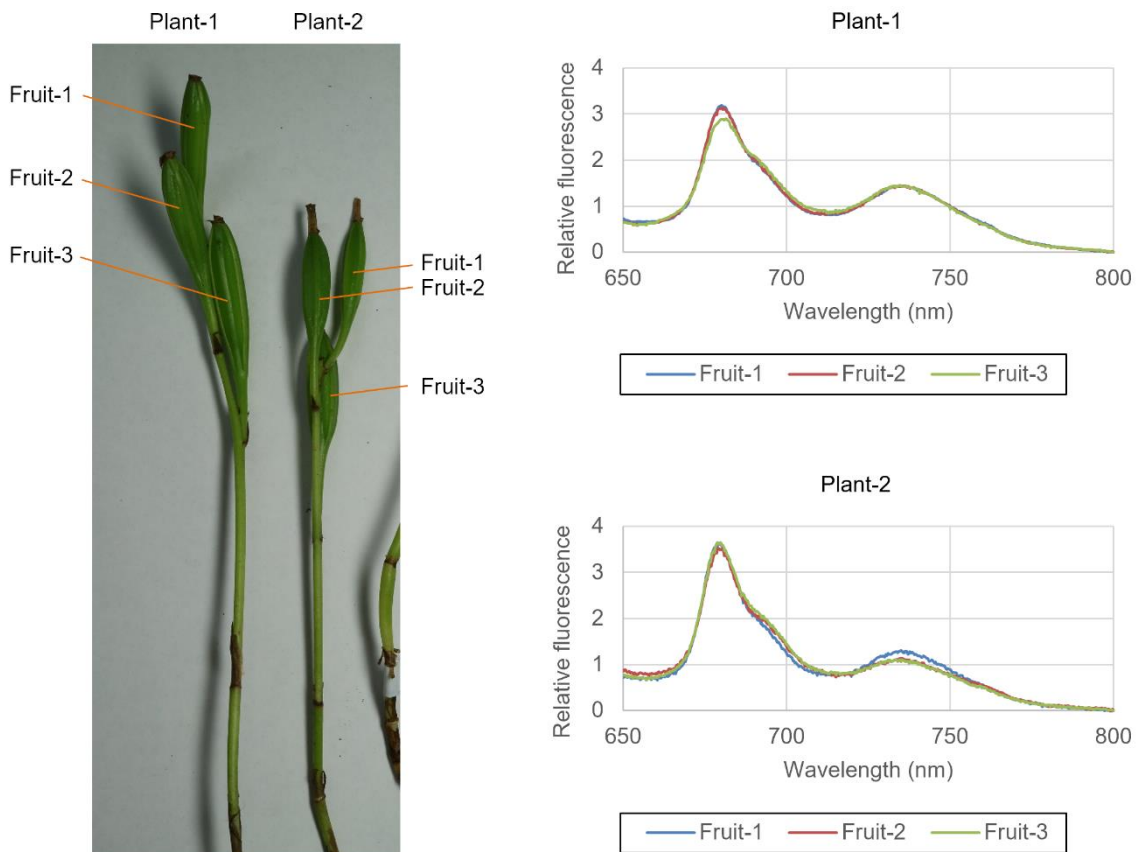
**Fig. S5** Comparison of Chl fluorescence at 77K among different fruits in a *C. macrorhizon* plant. Emission spectra of thylakoid membrane fractions from 3 different fruits of a plant were shown for two individuals.